Steel and Composite Structures, *Vol. 20, No. 4 (2016) 731-748*
DOI: http://dx.doi.org/10.12989/scs.2016.20.4.731

Strengthened and flexible pile-to-pilecap connections for integral abutment bridges

Jaeha Lee [1a], WooSeok Kim [*1], Kyeongjin Kim [1b], Soobong Park [2c] and Yoseok Jeong [2d]

[1] *Department of Civil Engineering, Korea Maritime and Ocean University, 727 Taejong-ro, Youngdo-gu, Busan, 606-791, Republic of Korea*
[2] *Department of Civil Engineering, Chungnam National University, 99 Daehak-ro, Yusung-gu, Daejeon, 305-764, Republic of Korea*

(*Received September 02, 2014, Revised January 12, 2015, Accepted May 13, 2015*)

Abstract. Pile-to-pilecap connection performance is important as Integral abutment bridges (IABs) have no expansion joints and their flexible weak-axis oriented supporting piles take the role of the expansion joint. This connection may govern the bridge strength and the performance against various lateral loads. The intention of this study is to identify crack propagation patterns when the pile-to-pilecap connection is subjected to lateral loadings and to propose novel connections for improved performance under lateral loadings. In this study, eight different types of connections were developed and modeled, using Abaqus 6.12 to evaluate performances. Three types were developed by strengthening the connections using rebar or steel tube: (i) PennDOT specification; (ii) Spiral rebar; and (iii) HSS tube. Other types were developed by softening the connections using shape modifications: (i) cylindrical hole; (ii) reduced flange; (iii) removed flange; (iv) extended hole; and (v) slot hole connection types. The connections using the PennDOT specification, HSS tube, and cylindrical hole were shown to be ineffective in the prevention of cracks, resulting in lower structural capacities under the lateral load compared to other types. The other developed connections successfully delayed or arrested the concrete crack initiations and propagations. Among the successful connection types, the spiral rebar connection allowed a relatively larger reaction force, which can damage the superstructure of the IABs. Other softened connections performed better in terms of minimized reaction forces and crack prevention.

Keywords: pile-to-pilecap connection; crack control; FEM; integral bridge

1. Introduction

Integral abutment bridges (IABs) have been successfully constructed and have served for three decades in the U.S. and Europe, due to their improved structural performance and low construction and maintenance costs. These benefits are gained due to the removal of the expansion joints and

*Corresponding author, Assistant Professor, E-mail: wooseok@cnu.ac.kr
[a] Assistant Professor, E-mail: jaeha@kmou.ac.kr
[b] Master's Student
[c] Master's Student
[d] Postdoctoral Researcher

http://www.techno-press.org/?journal=scs&subpage=6 ISSN: 1229-9367 (Print), 1598-6233 (Online)

substituting with flexible supporting piles.

Recently, the trend for the removal of expansion joints is presented in even longer bridges. In the U.S., both a 358 m long concrete girder IAB and a 318 m long steel girder IAB have been constructed and are now in service (Kunin and Alampalli 2000), with much longer bridges expected to be constructed with integral abutments. The lengthening of the IAB is mainly dependent on the supporting pile performance, i.e., the lateral displacement capacity of the supporting piles and the connection between the steel HP piles and the concrete pilecaps. Arsoy *et al*. (2002) conducted 75-year cyclic load testing under laboratory conditions for concrete piles, weak-axis oriented steel piles, and steel pipe piles, and concluded that the weak-axis oriented steel pile is a suitable choice for IABs because of its relative ductility and lower stiffness. Also, Abendroth *et al*. (2007) observed cracks in concrete piles of 33 m-long IAB although Gama and Almeida (2014) reported adequacy of concrete piles in IABs based on numerical studies. However, only limited research related to the weak-axis oriented steel pile-to-pilecap connection has been conducted, although numerous integral abutment bridge research studies have been completed and are still being carried out at the time of writing (Baptiste *et al*. 2011, Kim and Laman 2012, 2013, Kalayci *et al*. 2012, Civjan *et al*. 2013, Kim *et al*. 2014). Others (Ahn *et al*. 2011, Kim *et al*. 2012, Chacon *et al*. 2013) also numerically and experimentally investigated behavior of piles and girders separately.

Research related to IABs has focused on thermal movement and the soil-structure interaction between the soil and the supporting piles, backfill, and abutment (Kim and Laman 2010a, b). However, the pile-to-pilecap connection is one of the most vulnerable structural components of IABs due to lateral bridge movement caused by thermal effects and seismic loads (Baptiste *et al*. 2011, Ahn *et al*. 2011, Kim *et al*. 2013). Concrete pile to pile cap connection were studied by many researchers (Harries and Petrou 2001, Pam and Park 1990, Silva 1998), but steel pile to concrete pile cap connection studies were limited (Xiao *et al*. 2006, Xiao and Chen 2013). Nevertheless, currently no bridge design specification is available for the connection in AASHTO LRFD (2010) and PCI bridge design manual (2011).

Thus, the intention of this study is to identify crack propagation patterns when the pile-to-pilecap connection is subjected to lateral loadings, and to propose novel connections for improved performance under lateral loadings.

Previous studies showed that a spiral rebar strengthened connection significantly improves the performance of the connection when compared to a conventional or PennDOT rebar strengthened connection (Kim *et al*. 2013, Frosch *et al*. 2009, PennDOT 2007). It was found that the rebar can effectively control the crack propagation. However, the stiffness was increased, causing a relatively larger reaction force which will damage the superstructure of the IABs.

Therefore, the intention of this study is to develop a new pile-to-pilecap connection satisfying the ductility and low stiffness requirements compared to a conventional connection, to accommodate a 100 mm lateral displacement, which is equivalent to a 463 m-long concrete girder IAB or 347 m-long steel girder IAB. Additionally, a parametric study has been carried out for investigating the effects of spiral rebar geometries on the connection between the pilecap and pile.

In the U.S., a 358 m-long concrete girder IAB and a 318 m-long steel girder IAB were successfully constructed and are now in service. In this study, connections were firstly designed for large displacement and relatively large reaction force as the pilecap stiffness was increased. Subsequently, connections were designed for large displacements and small reaction forces in order to minimize possible girder and pile connection damages due to thermal displacement. Three different strengthened connection types with rebars (PennDOT, Spiral rebar type (SR) and HSS

tube type (HSS)) and five different types of connections without rebar (Cylindrical hole type (CH), Reduced flange type (RDF), Removed flange type (RMF), Extended hole type (EH) and Slot hole type (SH)) were studied. Detailed descriptions for the connection designs will be discussed in a later section.

2. Proposed pile-to-pilecap connection details

The benefits of using IABs are gained due to the removal of the expansion joints and substituting them with flexible supporting piles. However, currently, no bridge design specifications stipulate the rebar details for the pile-to-pilecap connection. PennDOT DM-4 4 (Fig. 1 (a)) specifies the rebar detail for the connection, but this detail was developed to compensate for down-drag force in the supporting piles. Spiral rebars (Fig. 1(b)) are easy to install and are proven to be very effective against seismic and lateral loads (Kim *et al*. 2013, Frosch *et al*. 2009). The proposed HSS tube connection (Fig. 1(c)) utilized the steel tube for the prevention of crack propagation. The removed flange detail utilized a modified shape of HP pile, where the embedded part of the flanges was removed and the steel plate is used to support the pilecap effectively. These three connections utilize rebars to strengthen the connection. In this study, this type of connection is called a "Strengthened connection" as indicated in Fig. 1. However, the stiffness of the strengthened connection was increased, causing relatively larger reaction forces. A large reaction force might damage the superstructure of the IABs. Therefore, another type of connection was developed. In this study, this is called the "Flexible connection", as indicated in Fig. 1. The flexible connection utilized the noble mechanical connections that were developed in this study, rather than using rebars. It allows certain amount of displacement at a local connection between the pile and concrete pilecap without generating large reaction forces. First, the flexible connection type is a cylindrical hole type (see Fig. 1(d), CH). The cylindrical hole embedded in the concrete pilecap prevents contact stress between the concrete and the flange edges of the HP pile, as shown in Fig. 1(d). A 40 mm diameter was considered in the CH type. The depth of the cylindrical hole was the same as the depth of the embedded part of the HP pile (450 mm).

Secondly, shape modification of the HP pile was considered. An HP pile with reduced flange (RDF) from 30 cm to 10 cm was used as shown in Fig. 1(e). The reduced flange allows a plastic hinge at the reduced section. Because a longer embedded depth showed a larger energy absorption capacity, the embedment length of the pile was also increased up to 600 mm from 450 mm. The reduced flange size was calculated in order to make a larger moment capacity in the concrete pilecap rather than in the HP pile. Accordingly, 33% of the original flange width was considered as a plastic hinge.

Thirdly, a removed flanged (RMF) HP pile was devised. The part of the flanges embedded in the concrete pilecap was removed in order to minimize the stress concentration, as presented in Fig. 1(f)). By removing the flanges, the stiffness of the connection and crack initiations were expected to be minimized and mitigated, respectively. To effectively resist axial forces transferred from the superstructure, 15 mm plates were also attached to the pile at the bottom of the concrete. The corner parts of the embedded web in the pilecap were cut off to reduce possible stress concentration that could cause another crack initiation. A single 900 mm long D19 rebar was also used at 150 mm below the top of the pile to prevent the pile from being pulled out due to down-drag forces.

Fourthly, an artificial gap was utilized in the connection EH. To artificially insert the gap

between the H-pile and the concrete pilecap, polystyrene was used to fill the gap (Fig. 1(g)). When the concrete is poured, due to the polystyrene, a gap between the pile and concrete pilecap will be formed. Since the polystyrene has a very small stiffness compared to the other construction materials, the polystyrene was neglected in the FE model. A 20 mm gap between the HP pile and

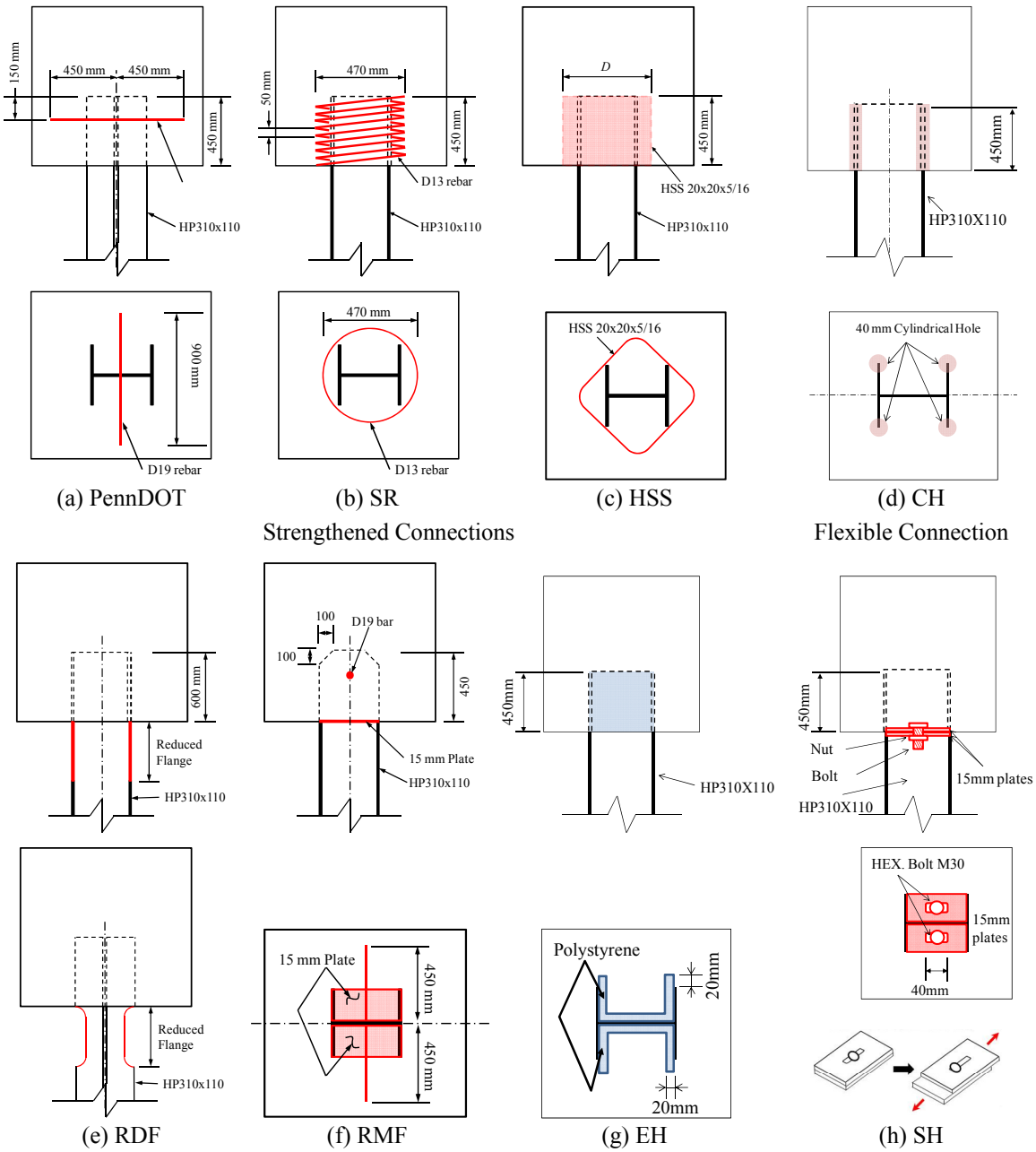

Fig. 1 Pile-to-pilecap connection type

the concrete pilecap was made in the model. The gap in the transverse direction was not considered and only the gap along the loading direction was considered. The other conditions are the same as those in the conventional connection.

Finally, similar to the extended hole details (EH, Fig. 1(g)), to insert the gap, a slot connection was utilized as shown in Fig. 1(h). The H-pile was cut into two parts: one part is the embedded part in the concrete pilecap and another is a part left exposed. Two separate HP piles are connected using a slot connection. In order to make a slot, two additional 16 mm thick plates were assumed to be welded to two cut surfaces of the HP pile. A 40 mm length of slot was placed into the two plates which are designed to be welded to the HP pile. The selected diameter for the bolt used in the slot was 18 mm.

3. Numerical analysis

A non-linear 3D numerical model was developed as shown in Fig. 2 by using ABAQUS 6.12 explicit. The superstructure rotational stiffness was considered as a rotational spring because its rotational capacity influences the pilecap rotation when it is subjected to the lateral displacement.

The backwall was modeled using beam elements to reduce the complexity of the model. The concrete pilecap was assumed to be a stub-type abutment which is typical in IABs, and was modeled using 3D non-linear solid elements.

Differential rotation at the construction joint between the superstructure and substructure as reported by Kim and Laman (2012) was also considered by using a calculated rotational stiffness in the model. Chore *et al*. (2014) and Conte *et al*. (2013) also proposed extensive numerical analysis methods for horizontally loaded piles. However, this study utilized the equivalent cantilever method proposed by Greimann and Wolde-Tinsea (1988) and Abendroth *et al*. (1989). Kim and Laman (2010b) also recommended to use the method to exclude nonlinear soil strata boundaries and to reduce computational costs. The equivalent cantilever model was experimentally evaluated by Girton (Girton *et al*. 1991) and was proven to be sufficiently accurate

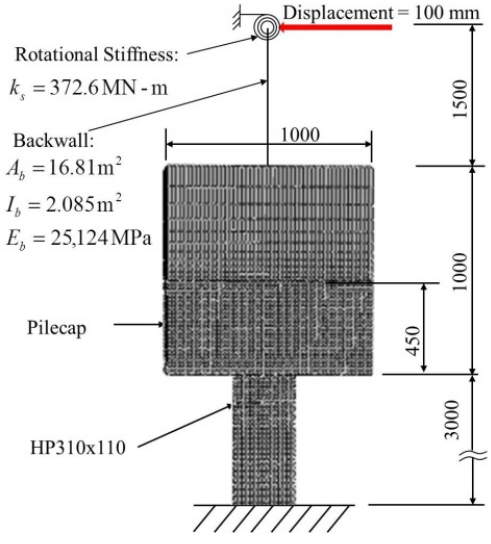

Fig. 2 Model developed for numerical analysis

for design purposes. PCI Bridge Design Manual (2011) also includes the equivalent cantilever method for laterally loaded pile design. In this study, the elastic modulus for concrete and steel are 21.76 GPa and 200 GPa, respectively.

In order to accurately predict the crack pattern, the damaged plasticity concrete model developed by Lee and Fenves (1998) was used. The Damage Plasticity model which was built in Abaqus has shown strong general solving capabilities for various concrete cracking behaviors. It provides a general capability for modeling concrete. It assumes non-associated multi-hardening plasticity and scalar damaged elasticity to model the irreversible damage. It allows user control of the stiffness recovery at the cracked region during cyclic load reversals. As a further study, other concrete material models such as the smeared cracking model should be used and the obtained results should be compared with the results in this study. The detailed theory could be found in an ABAQUS 6.12 user manual. For compressive behavior of concrete, Hognestad compression hardening curves were used and the tensional behavior of the concrete was determined based on recommendations of CEB-FIP (2010). The fracture energy of concrete was 126 N/m. The compressive strength and tensile strengths of the concrete were 20.68 MPa and 2.26 MPa, respectively. The yield strength of the rebar was 523 MPa. The model details for the rotational spring and backwall can be found in Kim *et al*. (2010b).

3.1 Model verification

FEM analysis results were compared with the experimental data by Frosch *et al*. (2009). The test specimen was secured to a strong floor using a clamping system. Axial and lateral loads were applied to the pile tip using a hydraulic machine. Detailed descriptions using the figures and test set up could be found in Frosch *et al*. (2009). The overall trends of the numerical analysis satisfactorily matched the experimental data, as presented in Fig. 3. The displacement was estimated with consideration of elastic deformations of the clamping rods under the applied load as described in Frosch *et al*. (2009). It should be noted that cyclic loads were applied in experimental conditions, while the FE analysis in this study only considered unidirectional displacement of the pile. Since the stress-strain relation of the concrete is relatively unique under the static condition according to Sinha *et al*. (1964), comparison of envelope of cyclic load-displacement curve with monotonic load-displacement is adequate.

A material model used in this study for concrete is the damage plasticity model built in Abaqus

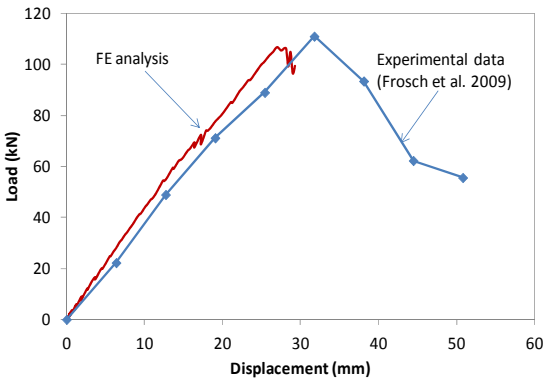

Fig. 3 Comparison of load-displacement graphs

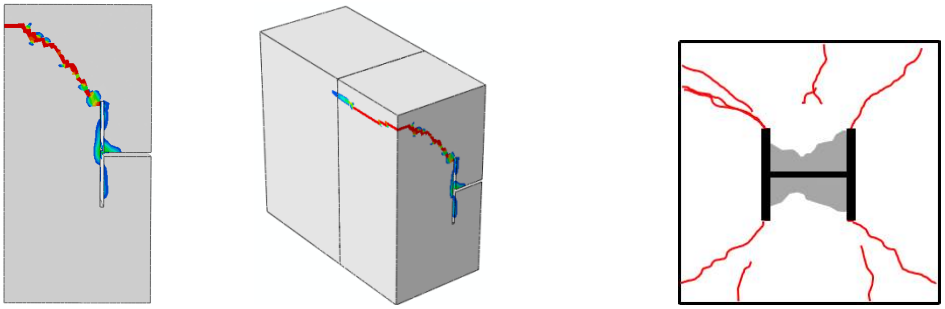

(a) Model result (b) Experimental result (Frosch *et al*. 2009)

Fig. 4 Comparison of crack pattern

commercial program. If the loads were applied in opposite direction repeatedly (cyclic loadings), fully damaged (cracked) and remained (not deleted) elements might affect the stiffness of the pile-to-pilecap connection; erroneous simulation results will be obtained. It was observed that the elements around the cracked regions were severely deformed after crack progression and reached up to the outer face of the pilecap. Therefore, after the cracking of the pilecap, the data was disregarded and was not plotted in Fig. 3.

The maximum forces which generated the complete cracks in the pilecap were approximately 111kN obtained from Frosch *et al*. (2009) compared to 107 kN in this study. The difference in load between the experiment and the predicted cases was within 4%. Similarly, the displacement difference between the experiment and the predicted cases was within 12% at maximum loads. In the experimental condition for structural tests, a deformation of the test frame due to the applied load can cause a possible additional gap between the supports and a loading point, which is a common situation. This could lead to an additional displacement to be added to the actual displacement. Therefore, the 12% difference in displacements was considered to be acceptable for model verification in this study.

Crack patterns were also well predicted as shown in Fig. 4. As explained earlier, cyclic loads were applied in experimental conditions, while the FE analysis in this study only considered unidirectional displacement of the pile. Therefore, crack propagations occurred in only one direction with the FE analysis. Based on the FEM results as shown in Fig. 4, the modeling methods and material models could be reliable for investigating pile-to-pilecap connections.

A preliminary study has investigated the possible crack patterns between the concrete pilecap and the steel pile using finite element analyses (Kim *et al*. 2013).

It was found that the crack patterns are sensitive to the boundary conditions specified in the simulation. It was concluded that depending on the abutment geometry and boundary conditions, i.e., abutment height, soil stiffness, pile sectional properties, etc., different crack patterns may occur. Therefore, in order to delay or minimize the crack occurrence, steel reinforcement should cover the four diagonal paths or the HP pile shape should be modified in order to mitigate crack occurrence.

Previous research proved that a spiral rebar could be used very effectively for delaying crack propagation (Kim *et al*. 2013). However, the large stiffness due to the addition of spiral rebars could cause a larger reaction force. Large reaction forces can damage the superstructure of IABs. Therefore, appropriate amount of the spiral rebar in the pilecap should be embedded to control the

overall behavior of the IABs under the thermal loading. In this study, a parametric study for shape and steel ratio of the spiral rebar had been investigated.

3.2 Analysis Results of Strengthened Connections (PennDOT, SR and HSS)

Obtained simulation results from strengthened connections such as PennDOT, SR and HSS types are shown in this section. Except SR, both PennDOT and HSS were not proven to be effective on strengthened connections. It is concluded that the performance of the SR detail is significantly higher than the PennDOT and HSS tube detail. Detailed information is as follows.

3.2.1 Obtained simulation results from PennDOT

Obtained analysis results from the PennDOT model are presented in Fig. 5. The crack initiation and propagation pattern was similar to the conventional case, as shown in Fig. 4. A complete pilecap crack was observed and this implies the pilecap body was split into two pieces due to cracks. Maximum stress in the rebar was approximately 33 MPa, which was only 11% of yield stress as shown in Fig. 5(c). After the complete pilecap crack at 61 mm displacement (Fig. 5(c)), maximum rebar stresses were 203 MPa (68% of yield stress). This implies that the PennDOT rebar is ineffective for mitigating crack initiation and propagation in the pile-to-pilecap connection. The D19 rebar was only used for preventing the pile from being pulled out due to down-drag forces. The maximum stress at D19 rebar was generated due to the down-drag forces.

3.2.2 Obtained simulation results from Spiral Rebar connection (SR)

As mentioned previously, a preceded research found that a spiral rebar is useful for delaying or arresting crack propagation (Frosch *et al*. 2009, Kim *et al*. 2013). However, a larger reaction force also could be generated if a steel ratio of the spiral rebar is massive. Accordingly, a parametric study on the shape and steel ratio of the spiral rebar (SR, Fig. 1(b)) was conducted in order to investigate the sensitivity of the pilecap behavior depending on the spiral rebar. Selected input parameters are the spacing between the pitch of the spiral rebar, diameter of the rebar and diameter of the spiral (width). Standard spiral rebar used in this study has 12.7 mm diameter of rebar, 50 mm pitch and 470 mm width. Observed output parameters are the load-displacement graphs of the pilecap and stress contour of the spiral rebars. Fig. 6 shows obtained results from the parametric study. Load-displacement graph was finished at the point of the cracking failure of the concrete pilecap.

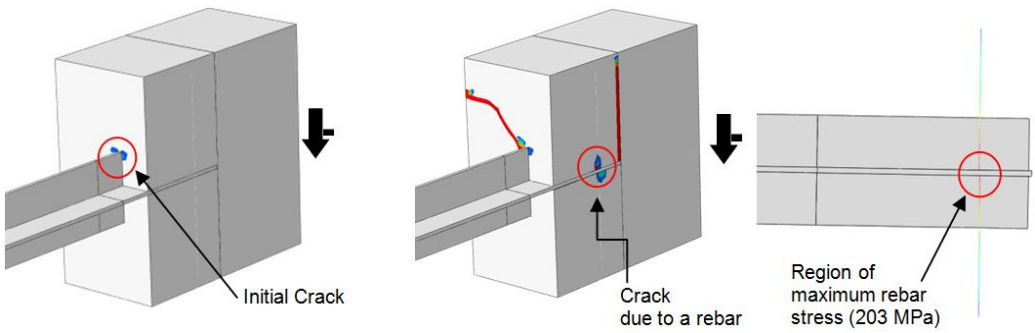

(a) Crack at Δ = 6.3 mm (b) Final crack at Δ = 61 mm (c) Rebar stress contour

Fig. 5 Crack location and stress in rebars (PennDOT)

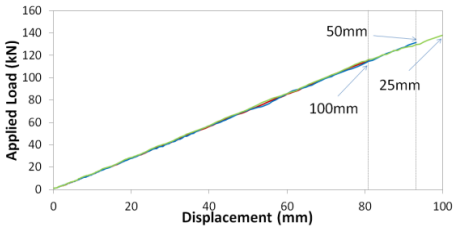

(a) L-D graph (spacing of the pitch)

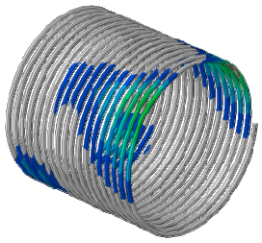

(b) Stress contour (Pitch: 25 mm)

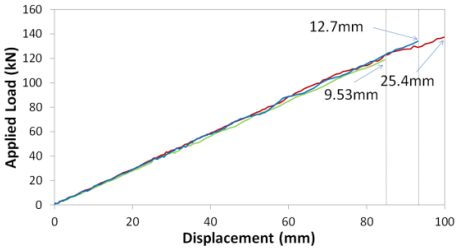

(c) L-D graph (diameter of the rebar)

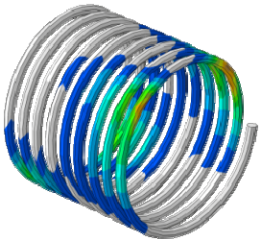

(d) Stress contour (Diameter of the rebar: 25.4 mm)

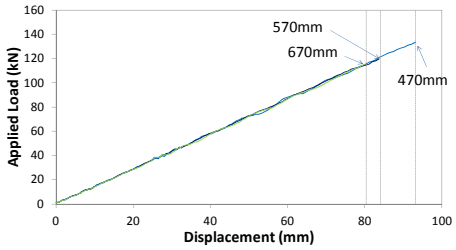

(e) L-D graph (diameter of the spiral)

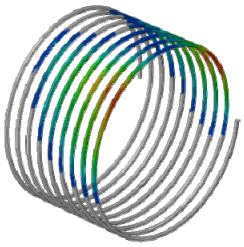

(f) Stress contour (Spiral width: 670 mm)

Fig. 6 Load-displacement graphs and stress contour of the various spiral rebar

As expected, the load-displacement behavior of the pile-to-pilecap connection under the lateral load was very sensitive to the geometry of the spiral rebar. As the spacing of the pitch is reduced from 100 mm to 50 mm and from 50 mm to 25 mm, the load carrying capacities of the pile-to-pilecap connections were increased up to 14.4% and 3.2% respectively (see Fig. 6(a)). Likewise, as the diameter of the rebar was increased from 9.53 mm to 12.7 mm and from 12.7 mm to 25.4 mm, the load carrying capacities of the pile-to-pilecap connection increased up to 10.2% and 0.8%, respectively (see Fig. 6(c)). Similarly, as the diameter of the spiral is decreased from 670 mm to 570 mm and from 570 mm to 470 mm, the load carry capacities of the pile-to-pilecap connection increased up to 5.6% and 10.9%, respectively (see Fig. 6(e)). This indicates that the three selected parameters are the key parameters for controlling the behavior of the pile-to-pilecap connection. Additionally, it shows that the increased load carrying capacities are not in linear relations with the selected parameters.

Furthermore, the spacing and aggregate sizes of the concrete could be determinants for properly designing the spiral rebar. Therefore, careful optimization procedures to properly design the shape and size of the spiral rebar depending on the geometry of the pilecap and concrete properties should be conducted for SR connection. Increased displacement capacities of various conditions

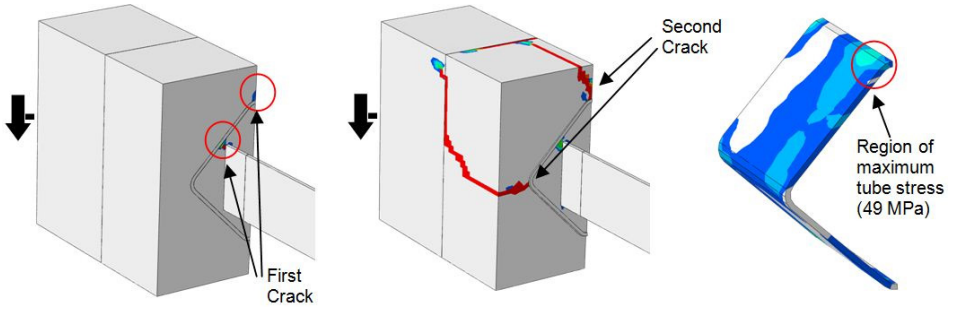

(a) Crack at Δ = 33 mm (b) Final crack at Δ = 55 mm (c) Tube stress contour

Fig. 7 Crack location and stress in HSS tube

could be the same as the results of the maximum applied load since the load-displacement graph shows approximately a linear line. In this study, the optimized size of the spiral rebar with 12.7 mm diameter of rebar, 50 mm pitch, and 470 mm width showed the best efficiency which could be considered as an optimized size and shape.

3.2.3 Obtained simulation results from HSS connection (HSS)

The obtained analysis results from the HSS model are presented in Fig. 7. The first crack was initiated from the corners of the HP pile as expected, and this crack was effectively arrested by the tube. Fig. 7(a) shows the crack at 33 mm of displacement. However, second cracks also occurred at locations other than the corner region of the HSS tube, resulting in earlier complete failure of the concrete pilecap (Fig. 7(b)) compared to that of conventional connection type (no rebar). It was found that both the rounded corner shape of the HSS tube and the shallow concrete cover depth between the tube and pilecap resulted in earlier crack failure. The maximum load at the complete pilecap crack was 83 kN, which is smaller than the conventional connection type (90 kN). The Von Misses stress of the tube obtained at maximum load was 49 MPa, indicating that the tube was ineffective in the pile-to-pilecap connection as shown in Fig. 7(c).

3.3 Analysis results of flexible connections (CH, RDF, RMF, EH, and SH)

Obtained simulation results from flexible connections such as CH, RDF, RMF, EH, and SH types are shown in this section. The CH type was found to be ineffective for connections. However, other types were proven to be effective for allowing large displacement without generating large reaction forces. Detailed information is as follows.

3.3.1 Compasrion of Cylinderical and Extended Hole connections (CH, EH)

Analysis results for the CH type are presented in Figs. 8(a) and (b). With the addition of the cylinderical holes, a complete crack occured at 60.34 mm displacement. This indicates that the CH did not effectively prevent the occurrence of the crack. It was found that the web of the HP pile pushed the concrete surface of the pilecap. Accordingly, stress concentration was generated at a local point of the cylinderical hole surfaces. The stress concentration at the cylinderical hole caused an early crack in the concrete pilecap. When the complete propagation of the crack occurred at 60.34 mm, the maximum stress in the HP pile was 298 MPa. The CH type is found to be ineffective for the pile-to-pilecap connection.

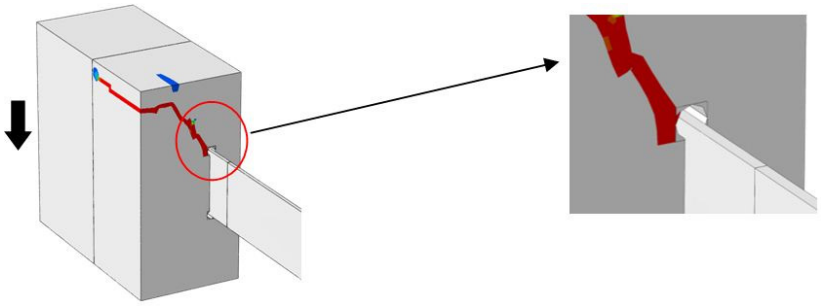

(a) Final crack at Δ = 60 mm (CH) (b) Zoomed view of CH (before contact)

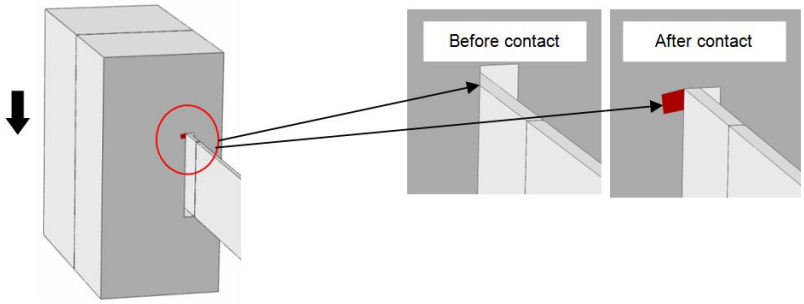

(c) Final crack at Δ=100 mm (EH) (d) Zoomed view of EH

Fig. 8 Crack locations in CH and EH

Analysis results obtained when using the extended hole details are shown in Figs. 8(c) and (d). Since the polystyrene was intended to be used between the concrete pilecap and the pile, a 20 mm gap was considered in the developed model. Unlike the CH type, in the HP pile, the pilecap and web have a 20 mm gap. Therefore, the contact stresses were not transferred to the concrete pilecap before the gap disappeared between the pile and pilecap. Thus, the reaction force was approximately zero until the 20 mm gap was closed. However, after this 20 mm displacement, both the pile and pilecap were in contact, resulting in a small crack on the contacted surface as shown in Figs. 8(c) and (d). However, this crack was not fully propagated, even under a displacement of 100mm. This indicates that the proposed connection of the EH could be used for mitigating cracks in the pilecap. The 20 mm gap between the pilecap and pile used in this study could be readjusted in order to allow a larger displacement. However, a larger gap might cause structural instability of the connection and a constructability issue. Therefore, a further study should be conducted in order to optimize the gap between the concrete pilecap and the HP pile. The calculated maximum stress of the HP pile at the contacted area was 55.9 MPa, which is much lower than the yield stress of the steel pile (400 MPa). At a displacement of 81 mm, plastic strain was generated at the fixed location of the H-pile, with no crack propagation being observed from the concrete pilecap.

It was found that the preformed gap should be used at both the flange and web of the HP pile. For example, the CH type that only has gaps at the flanges caused a stress concentration and resulted in early crack propagation of the pilecap.

3.3.2 Numerical analysis of RDM, RMF and SH

Analysis results for the RDM and RMF are presented in Figs. 9(a) and (b). Both types were

intended to be designed for a plastic hinge. Therefore, the plastic strained zone from both types were observed.

Figs. 9(a) and (b) show RDF analysis results. A crack propagation did not occur (Fig. 9(a)). Instead, a small crack initiation was observed near the flange of the pile. A plastic hinge was also formed at the pile as shown in Fig. 9(b). Plastic strain at 100 mm dispalmcent was 1.1%.

Figs. 9(c) and (d) show RMF analysis results. A small crack was observed from the side of the embedded web (Fig. 9(c)). Concrete cracks on the pilecap were not completely propagated at the full displacement of 100 mm (Fig. 9(c)). Since flanges were removed and the web was embedded in the centerline of the concrete pilecap, the stress concentrations that generally occurred at the pile edges (where the pile flanges and concrete pilecap were in contact) disappeared. Improved crack prevention performance and reduced reaction forces were observed when using the removed flange details. This implies that the removed flange details could be used for better energy absorption in pile-to-pilecap connection details under lateral loads. The rebar stresses were mostly concentrated at the connection between the web and the rebar due to the downwards force generated by the lateral movement. Plastic strain was also observed on the web of the pile located at the bottom surface of the concrete pilecap (Fig. 9(d)). However, fatigue resistance capacity of the removed flange should be further studied since plastic strains were formed at the thin plate (web of HP pile) and concentrated at the connection as shown in Fig. 9(d).

Fig. 10 shows SH analysis results. Analysis results obtained using the slotted hole connection details are shown in Fig. 10. Since the 40 mm slot was placed, 20 mm of displacement was allowed without any stress transferring to the concrete pilecap. However, after a displacement of

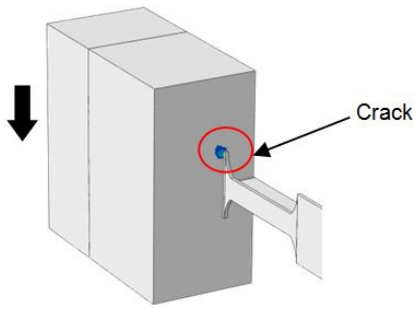

(a) Final crack at Δ = 100 mm (RDF)

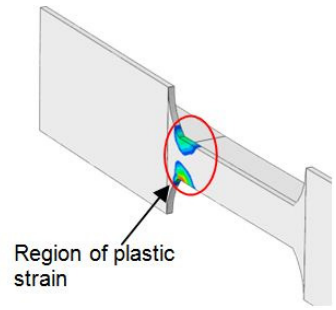

(b) Location of plastic strain (RDF)

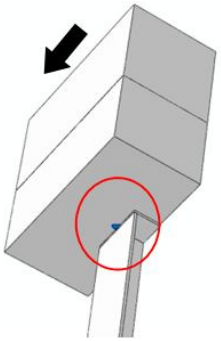

(c) Final crack at Δ = 100 mm (RMF)

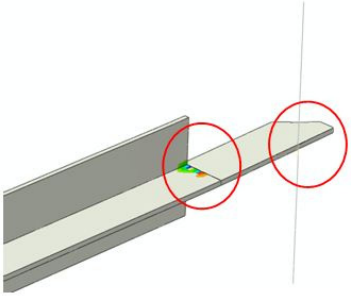

(d) Location of plastic strain (RMF)

Fig. 9 Crack locations and plastic strain in RDF and RMF

20 mm, the bolt and slot surface were in contact and the contact forces started to transfer. Finally, a small crack formed on the concrete side due to the contact stress under the 100 mm displacement as shown in Fig. 10(a). Fig. 10(b) shows the deformed shape after the contact. It was found that the plastic strain of the HP pile occurred at the slot connections but did not cause a crack in the concrete pilecap. Fig. 10(c) shows the stress contours in the HP pile before the contact. The obtained maximum stress for the HP pile before contact as shown in Fig. 10(c) was 0.06 MPa. After the contact had occurred, the maximum stress increased rapidly up to 16.96 MPa. The level of the stress was continuously increased up to the final 100 mm displacement. It should be noted that the plastic behavior of the bolts was not considered in this simulation. As previously mentioned, an 18 mm bolt diameter was used in this study. Stresses larger than the yield stress were generated from the bolting area as shown in Fig. 10(b). The stress level in the bolting area could be reduced by increasing the number of bolts and bolt size (diameter). Therefore, a further

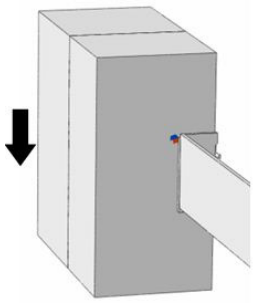

(a) Crack location

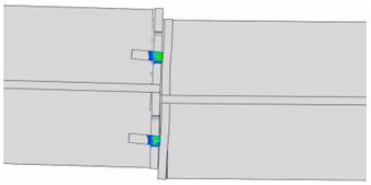

(b) Stress and slip at slot connection

(c) Stress contours of the pile before contact

Fig. 10 Crack patterns and stress contour of SH type

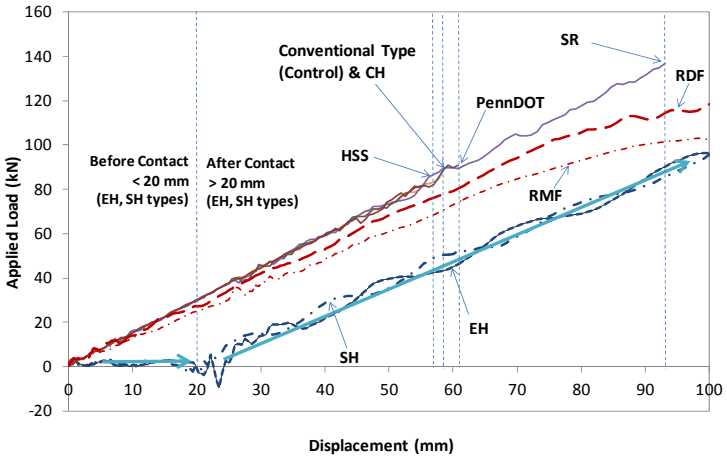

Fig. 11 Comparison of load-displacement graphs

Table 1 Comparison of obtained results of various connections

Connection Types	Displacement (mm)	Reaction force (kN)	Energy (kN-mm)
Conventional*	58	90	2610
PennDOT*	61	93	2827
SR*	93	137	6371
HSS*	55	83	2283
CH*	60	90	2614
RDF	100	120	6694
RMF	100	100	5940
EH	100	95	3987
SH	100	96	4022

*: Connection types failed by cracking before 100 mm displacement

study is needed in order to optimize the number and size of the bolts that connect the two plates of the HP piles. In this simulation, similar to the previous extended hole detail, a negligible crack was found at the contact area between the concrete pilecap and the HP pile. Therefore, the slotted hole connection could be a possible option for designing the pile-to-pilecap connection against large lateral displacements.

3.4 Comparions of load-displacment curves

Obtained load-displacement curves by Abaqus 6.12 explicit solver from each type were compared as shown in Fig. 11. Moving average smoothing algorithms were used to plot and compare the load-displacement graph. The calculated energies (area under the load-displacement curves), maximum loads, and displacements are also shown in Table. 1.

The PennDOT connection showed a similar performance (2827 kN-mm) to the conventional type. This indicates that the rebar used in the PennDOT specification was ineffective in controlling crack propagation. However, the SR connection exhibited 1.6 times higher strength and displacement compared to the conventional type. Because of the confinement by the spiral rebar, concrete cracks were delayed and strength was significantly increased. The energy absorption of SR was 6371 kN-mm. However, the stiffness was not changed.

The HSS tube type could not prevent crack propagation and allowed a large reaction force; thus, concrete crack failure occurred at a displacement of 56 mm. The connection failure occurred even earlier than the conventional connection. The first crack was initiated at the corners of the HP pile and seemed to be effectively arrested by the tube. However, secondary cracks abruptly developed from the corner region of the HSS tube, resulting in earlier cracking failure at a reaction force of 83 kN compared to the conventional type.

CH showed almost similar load-displacement behavior as the conventional type. Any improvement was observed from the preformed holes around the flange tip in the concrete pilecap.

The other proposed connections exhibited better performance to accommodate a 100 mm lateral displacement, which is equivalent to a 463 m-long concrete girder IAB or 347 m-long steel girder IAB, and all observed concrete cracks were negligible.

The RDF connection showed smaller energy and reaction force at 100 mm compared to the SR type. Among flexible connection types, the largest reaction force (120 kN) at 100 mm was

measured from the RDF connection. The reaction force of RDF could be reduced if a smaller percentage of the original flange width is considered as a plastic hinge. However, the structural stability and capacities under the vertical and lateral loads should also be checked.

The RMF connection showed even smaller energy compared to the RDF connection since a smaller reaction force was generated due to the effect of the plastic hinge formed at the removed flange section. The maximum reaction force at 100 mm displacement was 100 kN. The D19 rebar inserted for resisting the downwards force from the pile started to yield at a displacement of 98 mm and showed a plastic strain of 160 $\mu\varepsilon$ at 100 mm. The RMF connection acted as a plastic hinge, as intended.

Both the EH and SH connections showed no reaction forces up to a displacement of 20 mm because of the addition of the extended holes and slotted holes. However, after contact occurred, the reaction forces significantly and rapidly increased.

It should be noted that these simulations were conducted using explicit methods and quasi-static loading steps in order to save on the computational cost and avoid convergence problems that can occur in large deformation analyses of the composite materials with non-linear material properties. Therefore, after contact, a small impact was generated, causing oscillations in the extended hole and slot connection models as shown in Fig. 11. The oscillations were considered to be a negligible factor for the purpose of this study since the amplitude is small and FE results showed that the dynamic behavior does not affect the overall behavior of the pile-to-pilecap connection.

SR can take a larger energy of 6371 kN-mm, but it reached a full cracked condition at a displacement of 93 mm. Although other proposed connections such as RDF, RMF, SH and EH produced smaller energy absorption compared to the SR, these proposed connections can still displace the pilecap beyond a displacement of 100 mm with negligible cracking. Ductile and low stiffness pile-to-pilecap connections preventing cracks in the pilecap are the key to increasing the IAB length, to reduce the axial force in the superstructure and to allow a larger displacement without concrete cracking. This indicates that the proposed connection types with low energy absorption and larger displacement capacity can be successfully used in IABs against the large lateral displacement. SH and EH types showed smaller energy and displacements more than 100 mm. However, SH type may not be economical in practice. Therefore, RDF, RMF and EH types are recommended as the most suitable solution for increasing the IAB length among others.

4. Conclusions

The intention of this study was to develop new pile-pilecap connection types for IABs to improve bridge length, which is currently limited due to bridge thermal movement. However, the thermal movement capacity of the IABs could be improved by a better performing pile-to-pilecap connection which allowed larger displacements and lower reactions. To reduce stiffness and mitigate the four-way diagonal cracks from the HP pile, the use of rebars did not effectively improve the connection performance because the stiffness remained the same as the previous stiffness. In particular, the HSS tube and CH are not recommended because they caused equivalent or earlier complete cracking failure of the concrete pilecap compared to the conventional connection. Although rebars can effectively control crack propagation (e.g., SR), the stiffness was not reduced, causing a relatively larger reaction force compared to the flexible connections. Four types of flexible connection, including RDF, RMF, EH, and SH without rebars and one type of strengthened connection, SR, were proven to be effective under the lateral movement caused by

thermal variations. These developed flexible connections allowed displacement without generating relative larger reaction force and mitigated crack propagation. The following conclusions and recommendations could be derived from this study.

(1) The overall behavior of the developed models using Abaqus 6.12 explicit program with the concrete damage plasticity mode satisfactorily matched the experimental data.
(2) It was found that, using the developed models, the spiral rebar is very effective for controlling the crack propagation. The steel ratio and geometric shape of the spiral rebar was found to be a very sensitive parameter to control the behavior of the pile-to-pilecap connections.
(3) The HSS tube arrested the crack propagation from the first crack. However, at the same time, secondary cracks abruptly occurred, finally resulting in earlier failure and smaller energy absorption compared to the conventional connection.
(4) The CH type was demonstrated to be ineffective against lateral load. For the CH type, it was found that the web pushed the contacted surface of the pilecap, resulting in local stress concentration at the cylinderical hole surfaces. The stress concentration at the cylinderical hole caused an early crack in the concrete pilecap.
(5) Flexible connection types such as RMF, RDF, EH, and SH, without using spiral rebars, did not cause crack propagation and cracking failure.
(6) Having gaps between the pile and pilecap, the EH and SH connections successfully allowed a certain amount of displacement without generating a reaction force and structural instability. It is expected that these connections could also be applicable under the cyclic load on a daily basis; e.g., fatigue resistance.
(7) The absorbed energy generated at a 100 mm displacement of flexible connections was smaller than that of SR, and the proposed connections (RMF, RDF, EH, and SH) in this study performed better in terms of both minimized reaction forces and crack prevention.
(8) As a further study, a model sensitivity study with various concrete material models and contact properties is recommended.
(9) In this study, the equivalent cantilever pile length to exclude nonlinear soil strata boundaries was used. However, depending on the bridge abutment geometries and boundary conditions (i.e., abutment height and soil stiffness), different crack patterns may occur. Therefore, a soil-structure interaction analysis is recommended.
(10) Parametric studies for thickness and size of tube, cover depth of concrete pilecap, shape of tube, size of the bolt, and plate thickness are needed in order to optimize the proposed connection types.

Acknowledgments

This research was supported by the Basic Science Research Program through the National Research Foundation of Korea (NRF) funded by the Ministry of Education, Science and Technology (NRF-2012R1A1A044378).

References

Abendroth, R.E., Greimann, L.F. and Ebner, P.B. (1989), "Abutment pile design for jointless bridges", *J. Struct. Eng.*, **115**(11), 2914-2929.

Abendroth, R.E., Greimann, L.F. and LaViolette, M.D. (2007), "An integral abutment bridge with precast concrete piles", Final Report; IHRB Project TR-438.
Ahn, J., Yoon, J., Kim, J. and Kim, S. (2011), "Evaluation on the behavior of abutment-pile connection in tegral abutment bridge", *J. Construct. Steel Res.*, **67**(7), 1134-1148.
American Association of State Highway and Transportation Officials (AASHTO LRFD) (2013), AASHTO LRFD bridge design specifications, Washington, D.C., USA.
Arsoy, S., Duncan, J.M. and Barker, R.M. (2002), "Performance of piles supporting integral bridges", *J. Transport. Res. Board*, **1808**, 162-167.
Baptiste, K., Kim, W. and Laman, J.A. (2011), "Parametric Study and Length Limitations for prestressed Concrete Girder Integral Abutment Bridges", *J. Int. Assoc. Bridge Struct. Eng.* (*IABSE*): *Struct. Eng. Int.*, **21**(2), 151-156.
CEB-FIP (2010), CEB-FIP model code 2010, Bull. Inf. Com. Euro-Int.
Chacon, R., Mirambell, E. and Real, E. (2013), "Strength and ductility of concrete-filled tubular piers of integral bridges", *Engineering Structures*, **46**, 234-246.
Chore, H.S., Ingle, R.K. and Sawant, V.A. (2014), "Non linear soil structure interaction of space frame-pile foundation-soil system", *Struct. Eng. Mech., Int. J.*, **49**(1), 95-110.
Civjan, S.A., Kalayci, E., Quinn, B.H., Brena, S.F. and Allen, C.A. (2013), "Observed integral abutment bridge substructure response", *Eng. Struct.*, **56**, 1177-1191.
Conte, E., Troncone, A. and Vena, M. (2013), "Nonlinear three-dimensional analysis of reinforced concrete piles subjected to horizontal loading", *Comput. Geotech.*, **49**, 123-133.
Gama, D. and Almeida, J.F. (2014), "Concrete integral abutment bridges with reinforced conrete piles", *Struct. Concrete*, **15**(3), 292-304. DOI:10.1002/suco.201300081
Girton, D.D., Hawkinson, T.R. and Greimann, L.F. (1991), "Validation of design recommendations for intergral-abutment piles", *J. Struct. Eng.*, **117**(7), 2117-2134.
Greimann, L. and Wolde-Tinsea, A.M. (1988), "Design model for piles in jointless bridges", *J. Struct. Eng.*, **114**(6), 1354-1371.
Frosch, R.J., Kreger, M.E. and Talbott, A.M. (2009), *Earthquake Resistance of Integral Abutment Bridges*, FHWA/IN/JTRP-2008/11, Joint Transportation Research Program, Indiana Department of Transportation and Purdue University, IN, USA.
Harries, K.A. and Petrou, M.F. (2001), "Behavior of precast, prestressed concrete pile to cast-in-place cap connections", *PCI Journal*, **46**(4), 82-92.
Kalayci, E., Civjan, S.A. and Brena, S.F. (2012), "Parametric study on the thermal response of curved integral abutment bridges", *Eng. Struct.*, **43**, 129-138.
Kim, W. and Laman, J.A. (2010a), "Integral abutment bridge response under thermal loading", *Eng. Struct.*, **32**(6), 1495-1508.
Kim, W. and Laman, J.A. (2010b), "Numerical analysis method for long-term behavior of integral abutment bridges", *Eng. Struct.*, **32**(8), 2247-2257.
Kim, W. and Laman, J.A. (2012), "Seven-year field monitoring of four integral abutment bridges", *J. Perform. Construct. Facil.*, **26**(1), 54-64.
Kim, W. and Laman, J.A. (2013), "Integral abutment bridge behavior under uncertain thermal and time-dependent load", *Struct. Eng. Mech., Int. J.*, **46**(1), 53-73.
Kim, S., Yoon, J., Kim, J., Choi, W. and Ahn, J. (2012), "Structural details of steel girder-abutment joints in integral bridges: An experimental study", *J. Construct. Steel Res.*, **70**, 190-212.
Kim, W., Lee, J. and Jeoung, C. (2013), "Concrete crack control of pile-to-pilecap connection in integral abutment bridges under cyclic bridge movement", *Proceedings of the 3rd International Conference on Advanced Engineering Materials and Technology*, Zhangjiajie, China, May.
Kim, W., Laman, J.A. and Park, J.Y. (2014), "Reliability-based design of prestressed concrete girders in integral abutment bridges for thermal effects", *Struct. Eng. Mech., Int. J.*, **50**(3), 305-322.
Kunin, J. and Alampalli, S. (2000), "Integral abutment bridges: Current practice in United States and Canada", *J. Perform. Construct. Facil.*, **14**(3), 104-111.
Lee, J. and Fenves, L.G. (1998), "Plastic-damage concrete model for earthquake analysis of dams", *Earthq.*

Eng. *Struct*. *Dyn*., **27**(9), 937-956.
Pam, H.J. and Park, R. (1990), "Simulated seismic load tests on prestressed concrete piles and pile-pile cap connections", *PCI Journal*, **35**(6), 42-61.
Pennsylvania Department of Transportation (PennDOT) (2007), Design Manual Part 4, Structures: Procedures-Design-Plans Presentation, PennDOT Design 252 Manual Part 4, Commonwealth of Pennsylvania, Department of Transportation, Harrisburg, PA, USA.
Precast/Prestressed Concrete Institute (2011), PCI Bridge Design Manual, The PCI Bridge Design Manual Steering Committee, part of the Transportation Activities Council. ISBN: 978-0-9846705-4-3
Silva, P.F. (1998), "Experimental and analytical models to predict the response of pile to pile cap connections using simulated seismic loads", Ph.D. Thesis; University of California at San Diego, La Jolla, CA, USA.
Sinha, B.P., Gerstle, K.H. and Tulin, L.G. (1964), "Stress-strain relations for concrete under cyclic loading", *J*. *Am*. *Concrete Inst*., **61**(2), 195-212.
Xiao, Y. and Chen, L. (2013), "Behavior of model steel H-pile-to-pile-cap connections", *J*. *Construct*. *Steel Res*., **80**, 153-162.
Xiao, Y., Wu, H. and Yaprak, T.T. (2006), "Experimental studies on seismic behavior of steel pile-to-pile-cap connections", *J*. *Bridge Eng*., **11**(2), 151-159.

CC